A comparison of approaches to multi-body relative motion using the Kestrel CFD solver

H. Huang[1], M. Young[1], M. Giacobello[1] and R. Blyth[1, 2]

[1]Aerospace Division
Defence Science and Technology Group, Victoria 3207, Australia

[2]SKI Division
US Air Force SEEK EAGLE Office, Florida 32542, USA

Nomenclature

α	Angle of attack (°)
Δt	Time-step (s)
$\bar{c}$	Wing mean aerodynamic chord (m)
C_A, C_N, C_Y	Axial, normal and side force coefficient
C_{Mx}, C_{My}, C_{Mz}	Rolling, pitching & yawing moment coefficient
d	Subset distance (in)
D	Store diameter, model scale (1in)
L_δ	Inflation layer total height (0.138in)
T_{CPU}	CPU time per iteration (s)
y^+	Dimensionless wall distance

Abstract

The capabilities of Kestrel, a fixed-wing aircraft multi-physics simulation tool, were investigated by validation against a generic store release trajectory dataset. The release of the store was modelled using the overset capability within Kestrel using both unstructured and Cartesian background meshes. Kestrel generally produced results in agreement with the experimental data, with the Cartesian mesh showing slight improved agreement. Overall the angular displacements of the store were found to be more sensitive to the simulation setup, than the linear displacements.

Introduction

The wing-pylon-store (WPS) dataset is a comprehensive collection of experimental measurements obtained by the Arnold Engineering Development Complex (AEDC) for the purposes of validating computational fluid dynamics (CFD) simulations [3]. The wing-pylon-store has been the subject of several CFD comparisons over the years, including Lijewski and Suhs [4], Prewitt et al. [6], Eymann et al. [1], Loupy et al. [5], and Prior et al. [7]. These studies include both Euler and RANS simulations and, in general, the rotational displacements showed a greater sensitivity than the linear displacement to the simulation setup.

The wind tunnel setup comprised a wing-pylon and a generic store at 5% scale in a carriage configuration, as shown in Figure 1. The nominal tunnel condition was at a Mach number of 0.95 and a Reynolds number of 2.4×10^6 per foot. To simulate a trajectory within the facility a captive trajectory system (CTS) was employed, whereby a 6DOF integration of external forces was used to arrive at the store displacement. The store was ejected by two simulated constant forces (see Figure 1). After the store movement exceeded a full scale distance of 0.33ft, the ejector forces cease. The store trajectory was calculated on the assumption of a full-scale configuration at an altitude of 26 000 ft. Force and moment data were also collected for the store in isolation.

This dataset was used as a reference for comparison against CFD results from Kestrel v9, a fixed-wing aircraft simulation tool developed by the U.S. Department of Defense High Performance Computing Modernization Program (DoD HPCMP) [8]. Kestrel can solve both moving unstructured and Cartesian grids using a density-based implicit solver.

The capabilities of Kestrel were investigated in stages of increasing complexity. Firstly, the unstructured flow solver KCFD was applied to the case of a single unstructured grid. Secondly, the domain connectivity tool PUNDIT was employed by sub-setting the same unstructured grid and oversetting onto a background unstructured grid. Thirdly, the Cartesian solver SAMAir was assessed by replacing the background grid with an off-body Cartesian grid. Finally, the inbuilt 6DOF solver of Kestrel was assessed by enabling integration of aerodynamic forces, gravity and ejectors on the rigid store body.

All static cases were run on two configurations: with the isolated store in freestream, and with the store in the carriage position. An unstructured overset case with the 6DOF solver was also run.
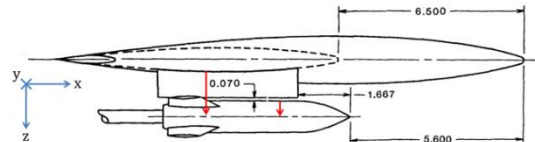

Figure 1: Wing-Pylon store dimension drawing in carriage configuration. Dimensions are in inches, with an indicative representation of the ejector force vectors in red.

Solution setup

Geometry and meshing

The geometries were meshed using Pointwise 18.1R1. Surface grids were triangulated with the Delaunay algorithm. Inflation layers were generated with a growth rate of 1.2 over a maximum of 30 layers from an initial height of $y^+ \approx 1$, giving a total inflation layer height of $L_\delta/D = 0.138$. Far-field extents were calculated using the mean aerodynamic chord length, $\bar{c}$, of the wing as the characteristic length. For unstructured and overset cases, the far-field boundary was represented as a sphere with radius of $40\bar{c}$. For Cartesian cases, the far-field comprised a square prism which extended a minimum of $40\bar{c}$ from all solid surfaces. A symmetry plane was employed for simulations in the carriage configuration. Figure 2 shows the surface grid and the off-body unstructured grid through the pylon centreline. In all cases the store sting was not modelled.

Flight condition

All numerical simulations were conducted at model-scale with Mach and Reynolds number matching to the experimental data. The reference static pressure was selected to achieve reference dynamic pressure equality to the AEDC CTS. The store masses, moments of inertia, gravitational

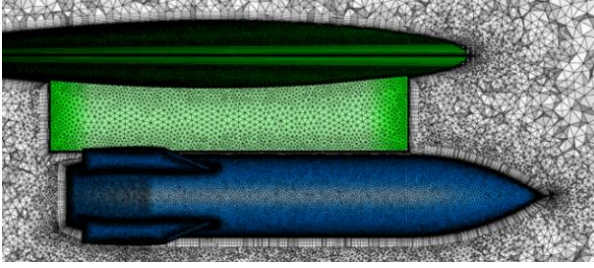acceleration and ejector forces were scaled to their equivalent full-scale properties.

Figure 2: The WPS in the carriage position in a single unstructured mesh

Numerical simulation

The Unsteady Reynolds-Average Navier-Stokes (URANS) equations were solved using second-order spatial and temporal discretisation. A time-step of $\Delta t = 10^{-4}$s was used, with 1 sub-iteration for static cases and 5 sub-iterations for dynamic cases. Turbulence was modelled with the Menter-SST model. Other turbulence models (SA, SA with rotational correction), the Menter 1-equation transition model and Quadratic Constitutive Relation for the Reynolds stresses (QCR) were tested and found to produce similar results. Both ejectors were modelled as external forces using distance-based cut-off criteria within Kestrel, which is consistent with the experimental approach (see [3], page 37 where the EJECT parameter is set to 2: *Distance function ejector forces and cutoff control*). All Cartesian cases were run with an off-body refinement threshold of 1 based on the shock sensor (a normalized value of the local velocity dotted with the pressure gradient) [1]. The finest Cartesian cells had edge length equal to the mean wall normal spacing across the overset boundary.

The computations were carried out on a Xeon 2.6 Ghz E5-2660 based system, with 300 CPU cores used for the store in freestream cases and 600 CPU cores for the carriage and release configurations.

Store in freestream

For all simulations of the store in freestream, the flight condition was at a nominal $\alpha = 6°$ to match test point 8 of Heim [3].

Figure 3 shows the spatial grid convergence of the unstructured meshes. As the nominal roll and yaw angles are zero and the store is symmetric about the *x-z* and *x-y* planes, C_Y, C_{Mx} and C_{Mz} are omitted for brevity. Convergence behaviour was overall monotonic, with exception of the finest mesh. The difference is likely due to the increasing aspect ratio of cells in the inflation layer from refinement. As the difference was small, the 7 million (M) cell mesh (see Figure 4 for visualisation) was selected for further assessment in the overset and Cartesian cases.

Using the URANS approach, the normal coefficient was under predicted, whilst the axial and pitch coefficients were over predicted. All coefficients fell outside of the experimental error bounds (shown in grey), but were found to agree with steady solutions from ANSYS Fluent using the Menter-SST turbulence model, and second order discretisation for all flow quantities. Future avenues of exploration for better matching of aerodynamic coefficients include a more detailed study of transitional URANS models and modelling effects of the store sting. A laminar solution

in Kestrel produced better results, reflecting concerns by Fox [2] regarding transition far aft of the model in the AEDC experiment.
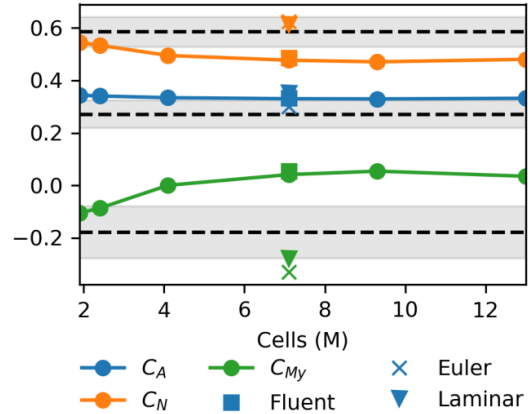

Figure 3: Spatial convergence of the unstructured mesh. The dashed line and grey band represent the experimentally measured value and uncertainty, respectively

Effect of subset distance for unstructured and cartesian background grids

Table 1 and 2 show the effects of subset distance on the aerodynamic coefficients for an unstructured and Cartesian background mesh, respectively. For the unstructured background mesh the effects of sub-setting distances were negligible above 0.5 store diameters. However, the effect of the overset did result in a small difference in the coefficients compared to the single unstructured mesh, especially for C_N and C_{My}. The causes may include interpolation between the store and background grids.

d/D	d/L_δ	C_A	C_N	C_{My}	T_{CPU} (s)
0.25	1.8	0.3509	0.5207	-0.0536	0.762
0.5	3.6	0.3445	0.5155	-0.0388	0.768
1.0	7.2	0.3453	0.5160	-0.0398	0.894
2.0	14.5	0.3431	0.5145	-0.0361	0.958
4.0	29.0	0.3426	0.5135	-0.0351	0.993
∞	∞	0.3304	0.4773	0.0407	0.753

Table 1: Effect of unstructured subset distance on aerodynamic coefficients and compute time. '∞' denotes a single unstructured mesh without oversetting.

d/D	d/L_δ	C_A	C_N	C_{My}	T_{CPU} (s)
0.25	1.8	N/A	N/A	N/A	N/A
0.5	3.6	0.3318	0.4696	0.0575	0.984
1.0	7.2	0.3308	0.4782	0.0378	0.841
2.0	14.5	0.3291	0.4775	0.0409	0.852
4.0	29.0	0.3294	0.4771	0.0413	0.878
∞	∞	0.3304	0.4773	0.0407	0.753

Table 2: Effect of Cartesian subset distance on aerodynamic coefficients and compute time. '∞' denotes a single unstructured mesh without oversetting.

For the Cartesian background mesh, the effects of subset distance were negligible above 2 store diameters, which was higher than the unstructured overset case. The simulation at 0.25 store diameters diverged, likely due to the interpolation of Cartesian cells within the inflation layer, as visualised in Figure 5. Overall the Cartesian background produced

coefficients which were closer to the single grid than those from an unstructured background.
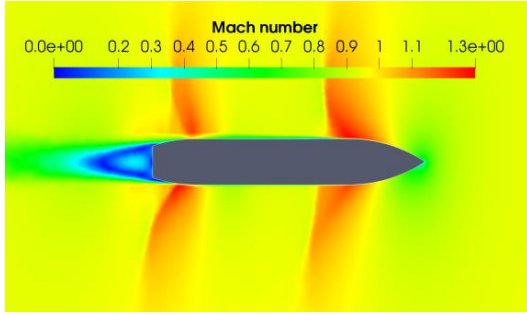

Figure 4: Mach number contours at $\alpha = 6°$ in the $y = 0$ plane
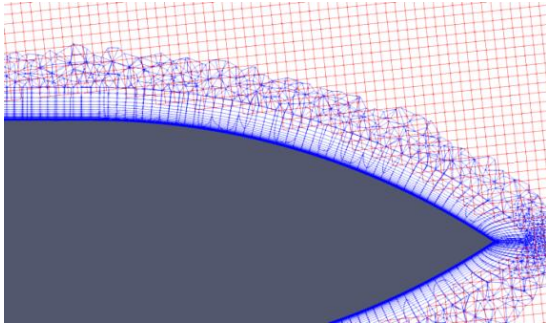

Figure 5: Cartesian off-body grid overset with the near-body inflation layer, $d = 0.25$ in

Carriage configuration

Due to the added complexity of the flow field when the store is in the carriage position, a grid convergence study was repeated. Figure 6 shows the spatial convergence of the unstructured mesh in carriage. Convergence behaviour was overall monotonic, with exception of the 15M cell mesh, which produced a different yaw coefficient. The underlying cause is unknown and merits further investigation. The 8M cell mesh was selected (see Figure 7 for visualisation) for further assessment in the overset and Cartesian cases. Most coefficients fell outside the error bounds of the experimental data, but exhibited overall agreement.
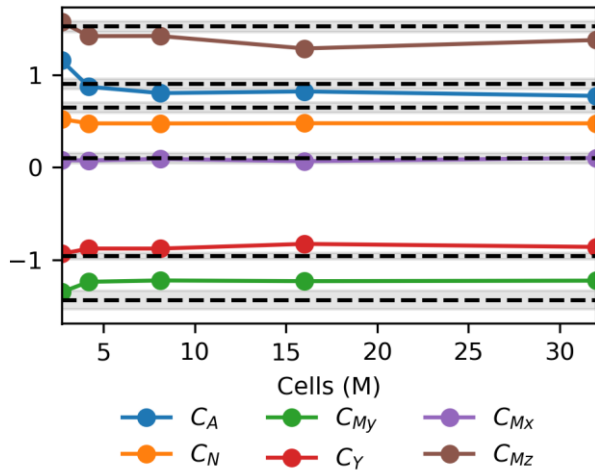

Figure 6: Spatial convergence of the unstructured mesh in carriage

Tables 3 and 4 show the effect of subset distance on aerodynamic coefficients for an unstructured background mesh. Unlike the configuration of the store in isolation, the coefficients converge for subset distances between 1 and 2 store diameters. This is likely due to increased complexity of the flow and also interfacing of the store and wing-pylon meshes within the boundary layer due to their proximity.
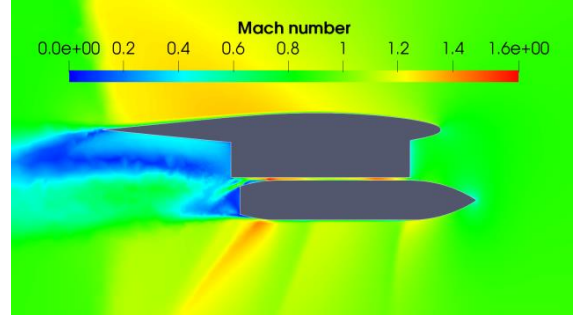

Figure 7: Mach number contours at carriage in the $y = 0$ plane

d/D	d/L_δ	C_A	C_N	C_{My}	T_{CPU} (s)
0.25	1.8	0.8188	0.4901	-1.2733	0.452
0.5	3.6	0.8084	0.4948	-1.2866	0.467
1.0	7.2	0.7936	0.4619	-1.1939	0.487
2.0	14.5	0.8024	0.4652	-1.2000	0.547
4.0	29.0	0.8017	0.4621	-1.1883	0.508
∞	∞	0.8020	0.4743	-1.2197	0.469

Table 3: Effect of unstructured subset distance on aerodynamic coefficients and compute time

d/D	d/L_δ	C_A	C_N	C_{My}	T_{CPU} (s)
0.25	1.8	N/A	N/A	N/A	N/A
0.5	3.6	0.8140	0.5220	-1.3418	0.641
1.0	7.2	0.8167	0.4827	-1.2445	0.638
2.0	14.5	0.8025	0.4804	-1.2298	0.584
4.0	29.0	0.8072	0.4773	-1.2225	0.465
∞	∞	0.8020	0.4743	-1.2197	0.469

Table 4: Effect of Cartesian subset distance on aerodynamic coefficients and compute time

Table 4 shows the effect of subset distance on the aerodynamic coefficients for a Cartesian background mesh. Similarly to the isolated store configuration, a small subset distance resulted in solution divergence, and likewise, the errors introduced by Cartesian oversetting were also significantly less than those from unstructured oversetting.

Store release trajectory

Before a full trajectory analysis was conducted, the model scale mass and length properties and 6DOF solver were validated by inputting the experimental aerodynamic coefficients as external forces in Kestrel. Figure 8 shows the pitch angle of the store as a function of time, and the sensitivity to the choice of time-step.

The time-step of $\Delta t \leq 1 \times 10^{-4}$s was required to obtain an acceptable agreement in pitch. It is also noted that the pitching moment was found to require the most restrictive time-step, as the ejector forces impart a large pitching

moment. Therefore, an accurate trajectory prediction requires resolving the ejector stroke termination with a time-step that is smaller than the time-step required to resolve purely aerodynamic motion.

The experimental trajectory was produced by modelling the ejector forces as acting in the body axis system, whereas the distance-based ejector in Kestrel only supports the parent axis system, or effectively the inertial axis system. However, given the strong agreement regardless, the 6DOF capabilities of Kestrel were considered successfully validated.
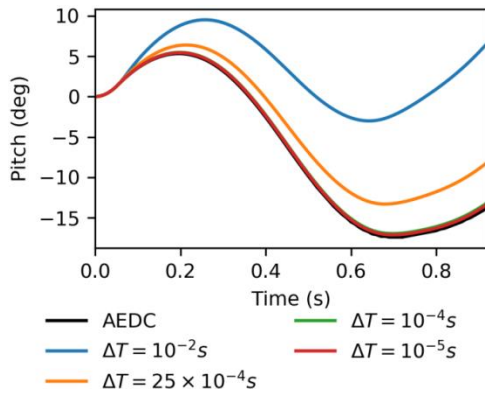

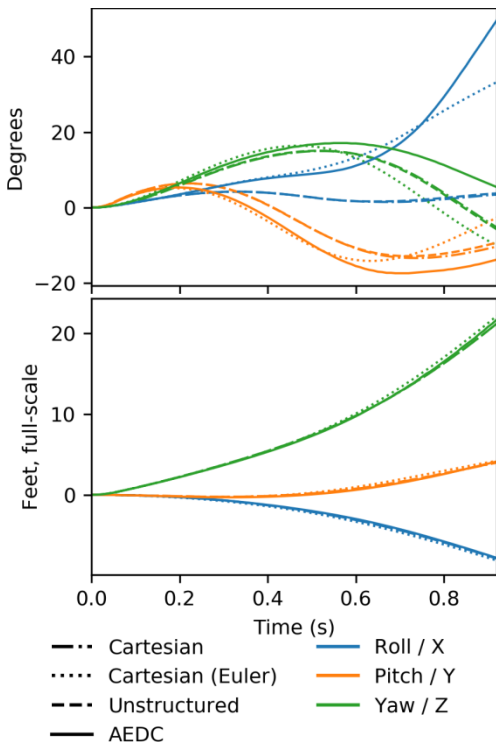*Figure 8: Sensitivity of trajectory pitch angle to simulation time-step*

Figure 9: Store trajectory rotational displacements (top) and linear displacements (bottom)

Final trajectory

Figure 9 shows the positional displacements and angular orientations of the store along the release trajectory. The displacements are matched well. Prediction of angular orientations followed the overall trends of the AEDC data, with exception of the roll angle. This is due to the small magnitude of the roll coefficient (see Figure 6), resulting in the roll coefficient sign being sensitivity to the simulation

setup. An Euler solution which predicted the sign of the roll coefficient differently resulted in a roll angle in general agreement to the experiment.

Conclusions

The capabilities of Kestrel were systematically assessed. KCFD and SAMAir produced results in agreement with the commercial solver ANSYS Fluent. In PUNDIT, oversetting of Cartesian cells to unstructured cells resulted in less error than oversetting unstructured cells on unstructured cells. Oversetting of Cartesian cells into inflation layers resulted in divergence. The 6DOF solver was found to be independently capable of accurately matching the AEDC store release trajectory.

Acknowledgements

References

[1] Eymann, T.A., Nichols, R.H., McDaniel, D.R. & Tuckey, T.R., Cartesian adaptive mesh refinement with the HPCMP CREATE-AV Kestrel Solver, *53rd AIAA Aerospace Sciences Meeting*, AIAA–2015–0040, 2015, https://doi.org/10.2514/6.2015-0040.

[2] Fox, J. H., *Generic Wing, Pylon, and Moving Finned Store*, Arnold Engineering Development Center, 2000.

[3] Heim, E. R., *CFD/Wing/Pylon/Finned Store Mutual Interference Wind Tunnel Experiment*, United States Air Force, 1991.

[4] Lijewski, L.E. & Suhs, N.E., Time-accurate computational fluid dynamics approach to transonic store separation trajectory prediction, *J. Aircraft.*, 36, 4, 1994, 886-891, https://doi.org/10.2514/3.46575

[5] Loupy, G.J.M., Barakos, G.N. & Taylor, N.J., Store release trajectory variability from weapons bays using scale adaptive simulations, *AIAA Journal*, 56, 2, 2018, 752–764, https://doi.org/10.2514/1.J056485.

[6] Prewitt, N.C., Belk, D.M. & Maple, R.C., *Multiple-body trajectory calculations using the beggar code,' J. Aircraft*, 36, 5, 1999, 802–808 https://doi.org/10.2514/2.2513

[7] Prior, M.A., Kernazhitskiy, S.L. & Jolly, B., 'Assessment of HPCMP CREATEAV Kestrel version 7.1.2 accuracy for store separation simulations,' *AIAA 2018 Applied Aerodynamics Conference*, AIAA-2018-4123, https://doi.org/10.2514/6.2018-4123.

[8] US DoD (2018). *CREATE Air Vehicles*, https://www.hpc.mil/index.php/2013-08-29-16-03-23/computational-research-and-engineering-acquisition-tools-and-environments/create-air-vehicles-av